DOI: 10.1002/adma.200602872

The Direct Patterning of Nanoporous Interlayer Dielectric Insulator Films by Nanoimprint Lithography**

By *Hyun Wook Ro*, *Ronald L. Jones*, *Huagen Peng*, *Daniel R. Hines*, *Hae-Jeong Lee*, *Eric K. Lin*, *Alamgir Karim*, *Do Y. Yoon*, *David W. Gidley*, and *Christopher L. Soles**

Nanoimprint lithography is emerging as a next-generation patterning technique with enormous potential.[1–14] The technology combines the inherent compatibility of a stamping process for high volume manufacturing with a patterning resolution comparable to electron beam lithography. There are many examples of features 10 nm and smaller fabricated via imprint technologies.[4–7] More recently, nanoimprint lithography has been attracting attention for reasons other than resolution and throughput. It is also capable of replicating complex multi-level or 3D patterns in a single imprint.[7–11] Incumbent optical lithography requires multiple patterning steps to fabricate multi-level structures. Nanoimprint lithography also has the potential to directly pattern a range of materials, not just sacrificial resists that must then be combined with additive or subtractive processes to transfer the pattern into a functional material. The ability to directly pattern complicated structures into functional materials without photoresists, etching, or deposition has the potential to greatly simplify device fabrication and reduce manufacturing costs.[8–11]

There is an interest in directly patterning spin-on silsesquioxane materials,[10–14] especially for their use as interlayer dielectrics (ILDs) in semiconductor interconnect structures.[10,11] Current microprocessors require eight or more layers of wiring in the interconnect structure to pass the electrical signals into and out of the transistor gates. Optical lithography routes based on the dual damascene method require approximately 20 processing steps for each of these layers and it has been suggested that imprinting the low-dielectric constant (low-k) material with a two-tier mold that produces via and trench structures in a single imprint has the potential to cut the lithography steps in half.[10,11] Directly patterning the dielectric insulator would also eliminate multiple etching and polishing steps, thereby greatly simplifying device fabrication.

ILD materials today, which are used in their dense form, have dielectric constants (k) on the order of $k \approx 2.9$. Next generation devices will require ILDs with an ultralow-k ($k < 2.3$) to minimize the cross-talk between adjacent interconnect lines, decrease power consumption, and decrease the resistance-capacitance (RC) delay in the circuit response. This can only be realized by introducing large quantities of nanoscale porosity into the ILD material.[15–19] The imprint literature on this topic thus far has been limited to qualitatively demonstrating the feasibility of patterning non-porous low-k materials.[10,11] Here we make the crucial jump to create a *nanoporous* low-k pattern at or near the ultralow-k constant of $k \approx 2.3$ and quantify the fidelity of the pattern transfer process with nm precision.

In addition to dielectric performance, candidate ILD materials must satisfy several other criteria. In particular, they need to have a suitable elastic modulus ($E > 6$ GPa) and display a low coefficient of thermal expansion ($\mathrm{CTE} < 30 \times 10^{-6}\,^{\circ}\mathrm{C}^{-1}$). Elsewhere we have developed a poly(methylsilsesquioxane) (PMSQ)-based terpolymer (a copolymer of methyltrimethoxysilane, 1,2-bis(triethoxysilyl)ethane, and dimethyldimethoxysilane) optimized to meet many of the required properties for an ILD material, including a dielectric constant of 2.84 ± 0.05 measured at 1 MHz, a Young's modulus of (10.5 ± 0.5) GPa,[18,19] and a coefficient of thermal expansion of $(19.2 \pm 1.7) \times 10^{-6}\,^{\circ}\mathrm{C}^{-1}$. We suspect that the relatively high modulus of this material will be an important factor for retaining the structural integrity of a porous imprinted nanostructure. This material is rendered porous by adding a PEO-*b*-PPO surfactant (Tetronics, T150R1) as the porogen. The porogen volatilizes from the PMSQ network between 300 and

[*] Dr. C. L. Soles, Dr. H. W. Ro, Dr. R. L. Jones, Dr. H.-J. Lee, Dr. E. K. Lin, Dr. A. Karim
NIST Polymers Division
100 Bureau Drive, stop 8541, Gaithersburg, MD 20899 (USA)
E-mail: csoles@nist.gov
Dr. H. Peng, Prof. D. W. Gidley
Department of Physics, University of Michigan
Ann Arbor, MI 48109 (USA)
D. R. Hines
Laboratory for Physical Sciences, University of Maryland
College Park, MD 20740 (USA)
Prof. D. Y. Yoon
Department of Chemistry, Seoul National University
Seoul 151-747 (Korea)

[**] Official contribution of the National Institute of Standards and Technology; not subject to copyright in the United States. The error bars presented throughout this manuscript indicate the relative standard uncertainty of the measurement. Certain commercial materials and equipment are identified in this paper in order to specify adequately the experimental procedure. In no case does such identification imply recommendation by the National Institute of Standards and Technology nor does it imply that the material or equipment identified is necessarily the best available for this purpose. This work was supported in part by the System IC 2010 Project of Korea, the Chemistry and Molecular Engineering Program of Brain Korea 21 Project, and the NIST Office of Microelectronics Programs. We also acknowledge the Nanofabrication Laboratory in the NIST Center for Nanoscale Science and Technology (CNST) for the use of their facilities. Supporting Information is available online from Wiley InterScience or from the authors.

ADVANCED MATERIALS

400 °C, leaving nanoscopic pores in its place. Increasing the porosity by increasing the porogen loading is an effective way to reduce the dielectric constant of the ILD material.

The densities of smooth, fully vitrified PMSQ terpolymer films are characterized with specular X-ray reflectivity (SXR). Figure 1a shows a series of SXR curves as a function of the porogen loading. At low Q there is a critical wave vector, Q_c as indicated by the arrow, below which total reflection of the incident X-rays occurs ($\log(R) = 0$); beyond Q_c there is a pronounced reduction in the reflectivity. The square of this critical wave vector is directly proportional to the density of the film. A second Q_c occurs at slightly higher Q, corresponding the Q_c of the underlying silicon substrate. As the porogen concentration increases the first Q_c shifts to lower wave vectors indicating a reduced density of the film, consistent with the generation of porosity. The dielectric constants of these films were characterized using a metal-insulator-metal test structure at a frequency of 1 MHz. Figure 1b show the corresponding k as a function of Q_c^2. As expected, k increases linearly with density. The film with $Q_c^2 = 4.64 \times 10^{-4}$ Å^{-2} meets the target dielectric value of $k = 2.3$, corresponding to a porogen loading of 20 % by volume. Positron annihilation lifetime spectroscopy measurements on this film indicate that the pores have an average diameter of roughly 2.2 nm, verifying the nanoscale dimensions of the porosity. Now we quantify how this ultralow-k material responds to nanoimprint lithography patterning. For comparison, we also imprint a nonporous (porogen-free) version of this material. The details of the nanoimprint lithography patterning procedures are described in the Experimental Section.

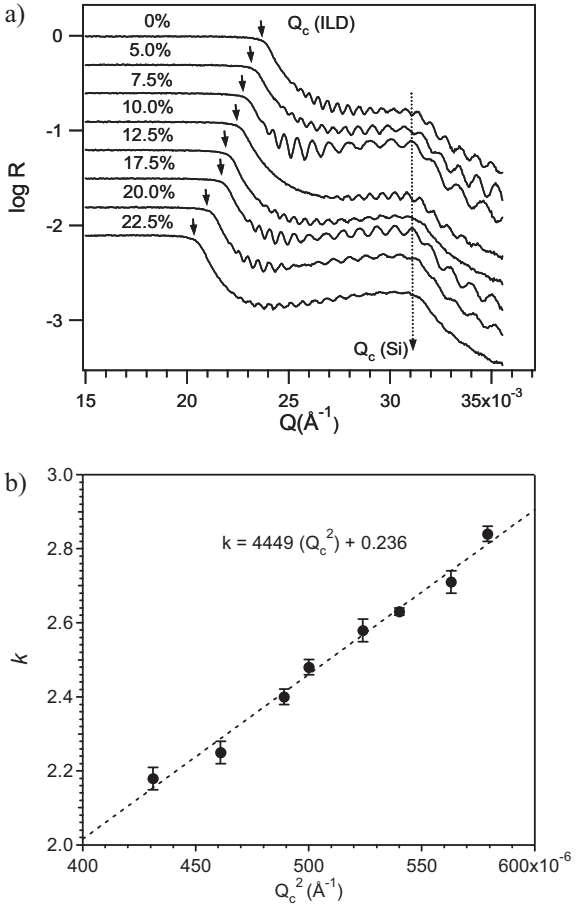

Figure 1. Specular X-ray reflectivity curves are shown in part (a) for a series of unpatternred PMSQ-based terpolymer films as a function of the porogen loading (the volume % porogen is indicated). Except for the 0 % porogen loading, the curves have been vertically offset for clarity. The critical angle Q_c for the film, indicated by the arrow, systematically shifts to lower Q with higher porogen content, indicating a decrease in the film density. In part (b) a linear correlation is observed between the Q_c^2 of the film and the experimental dielectric constant (k).

SXR can be used to quantify the pattern height, the residual layer thickness and the line-to-space ratio of parallel line-space gratings patterns, as described elsewhere in detail.[20,21] Figure 2a shows the SXR data for the imprinted films, both with and without the porogen, after imprinting but before vitrification. Now a series of three Q_cs, not two as in Figure 1a, are observed suggesting three layers of distinctly different density in the sample. As described elsewhere[20,21] these three layers in order of increasing Q_c (increasing density) correspond to the region of the patterned dielectric material, a residual layer beneath the patterns, and the supporting Si substrate. Fitting the reflectivity profile with a multilayer recursive algorithm based on the formalism of Parratt[22,23] reveals the density profile as a function of distance through the patterned region, the residual layer, and the supporting substrate.

Figure 2b shows the density profiles from the fits to the reflectivity data in part (a). Here the density is displayed on the horizontal axis in units of Q_c^2 (the scattering length density, SLD) while the distance z is displayed on the vertical axis. Annotations to Figure 2b help orient the density profile with the physical features of the pattern. The total height for the imprint of the porogen-free sample is (1603 ± 10) Å with residual layer thickness of (766 ± 10) Å. For the porogen-loaded film the pattern height and residual layer thickness are (1600 ± 10) Å and (757 ± 10) Å, respectively. Within the uncertainty the imprinting process appears to be reproducible; with or without porogen the same profile is obtained. Notice, however, that the density profile in the region of the patterned height is not vertical. The effective density is greater near the residual layer and decreases towards the top of the patterns, indicating that the pattern is tapered or slightly wider near their base. By comparing the Q_c^2 values in the patterned region to the Q_c^2 values of the residual layer ($Q_c^2 = 6.0 \times 10^{-2}$ Å^{-2}), one can calculate the average line-to-space ratio as a function of pattern height. A series of horizontal lines labeled "l" and "s" superimposed on the profiles to indicate the relative magnitude of the line and space widths at a few different heights in the patterned region.

After imprinting and demolding, the imprinted patterns were converted into a fully vitrified structure by thermal curing at 430 °C for 1 h in an inert nitrogen environment. Figure 2c shows the SXR data before and after vitrification for the porogen-free and porogen-loaded patterns. Once again

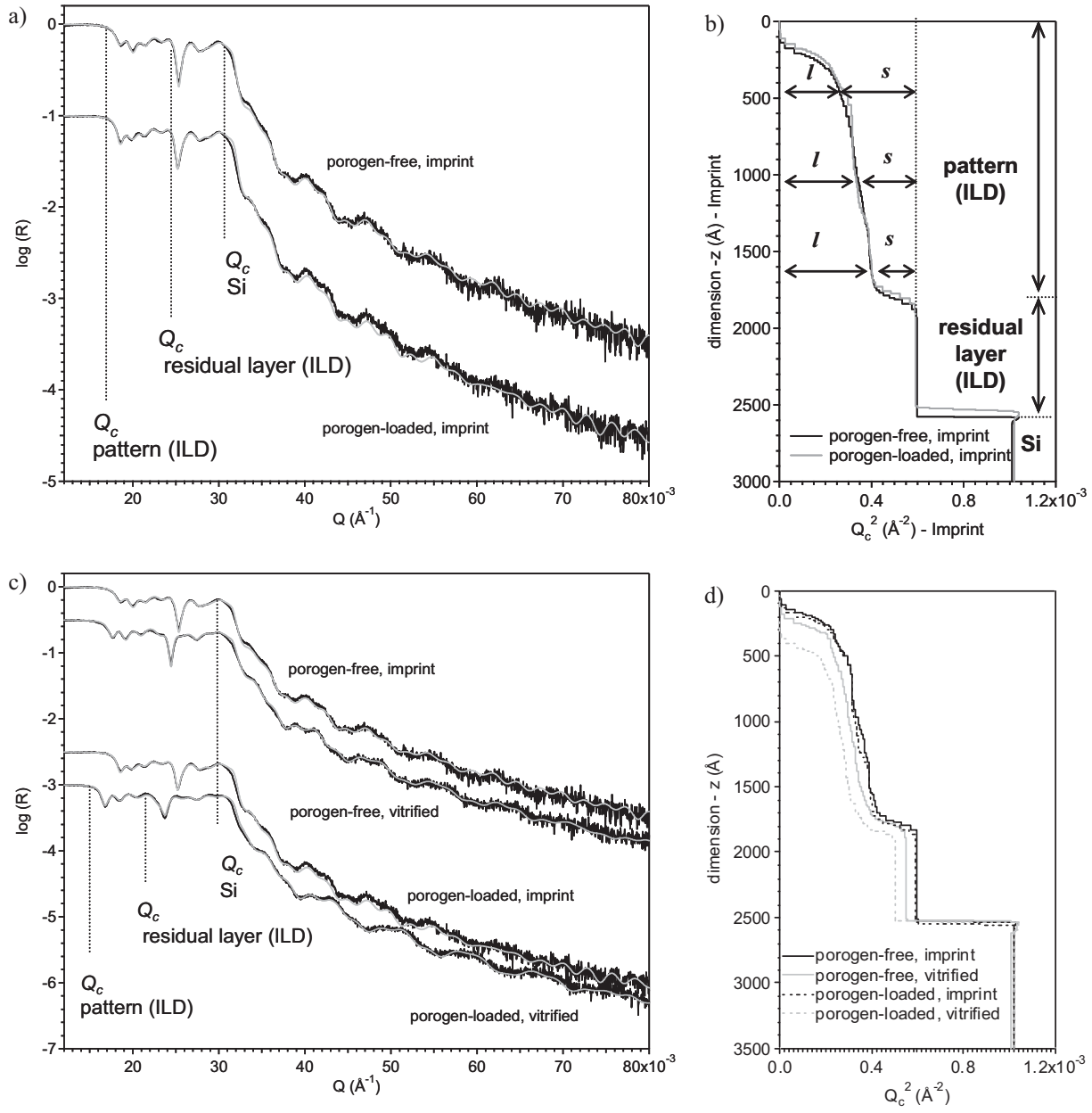

Figure 2. The reflectivity data and scattering length density (SLD) profiles are shown for the different stages of the patterning process. Part (a) shows the raw reflectivity data (black) for the as-imprinted patterns of both the porogen-free and porogen-loaded samples. Part (b) shows the SLD profiles corresponding to the fits in Part (a). The annotations indicate which portions of the profile correspond to the different layers in the sample. In the patterned region, a three pairs of lines labeled "*l*" and "*s*" are drawn to help illustrate how the line-to-space ratio can be determined. At a given height *z*, the ratio of *l* to *s* is precisely equal to the line-to-space ratio at that height. In parts (c) and (d) the same reflectivity data and SLD profiles are repeated after vitrification, respectively.

a series of three Q_cs are observed corresponding to the patterned region, the residual layer, and the supporting Si substrate. The Q_c of the Si substrate does not change upon vitrification, as expected, while the Q_cs of the patterned region and residual layer shift to lower Q. This low Q shift is more pronounced in the porogen-loaded sample owing to the generation of the porosity; the density is significantly reduced. The small change in Q_c for the porogen-free sample reflects the creation of a small amount of inherent microporosity, common for the vitrification of PMSQ-type materials.

Figure 2d displays the corresponding density profiles from the fits to the experimental reflectivity data in part (c). Consistent with Figure 2b the density profiles for the as-imprinted porogen-free and porogen-loaded samples overlap. After vitrification, the pattern heights shrink by approximately 4.0 % and 12.0 % in the porogen-free and porogen-loaded

ADVANCED MATERIALS

samples, respectively. In contrast to these results, the residual layer thickness shrinks approximately 3.0 % and 9.0 % for the porogen-free and porogen-loaded samples, respectively. For some reason, greater vertical shrinkage occurs in the patterned region, especially for the porogen-loaded sample. One also notices an overall reduction of the apparent density (uniform shift to smaller Q_c^2 values) throughout both the patterned region and the residual layer after vitrification; the porogen-free and porogen-loaded profiles no longer overlap. There are two possible explanations. The first is the generation of porosity (reduced density) without lateral shrinkage, where the line-to-space ratio stays the same. The second would be a lateral shrinkage where the line width decreases and the space or gap width increases but the density of the material stays the same. SXR measurements alone are unable to distinguish between these two scenarios because, as discussed previously,[20,21] the in-plane directions are relative in terms of a line-to-space ratio; only the vertical or height dimension are absolute from SXR.

To resolve the uncertainties in the pattern widths and densities, critical dimension small-angle X-ray scattering (CD-SAXS) is needed to quantify the pattern widths and/or periodicities.[24,25] These measurements are described in detail in the supplemental information, but here it is sufficient to note that the periodicity of (1970 ± 10) Å remained constant (and equal to the mold dimensions) for all samples and the line widths did not change appreciably. From this absolute lateral length scale, it is possible to convert the density profiles or line-to-space ratios in the patterned region of Figure 2b and d into absolute pattern width variations as a function of the pattern height, i.e., define the pattern cross-section.[21] Figure 3 shows the full pattern cross-sections for all the samples, compared with the cross-section of the imprint mold (also obtained by a combination of SXR and CD-SAXS) to quantify the fidelity of the pattern transfer process. In parts (a) and (b) of Figure 3, a fairly isotropic shrinkage of approximately 5 to 10 % relative to the mold is evident in the as-imprinted patterns for both the porogen-free and the porogen-loaded samples. As discussed with respect to Figure 2b, this degree of shrinkage is independent of whether the sample contains porogen or not. A small amount of shrinkage in these samples after imprinting is reasonable. The as-cast films will retain a fraction of the residual spin coating solvent. Imprinting at 200 °C under a vacuum should help liberate this residual solvent and lead to shrinkage. The material will also partially cross-link at 200 °C, consistent with some shrinkage.

Figure 3c and d quantify how vitrification after imprinting affects the shape of the porogen-free and porogen-loaded patterns, respectively. As discussed previously in Figure 2d, an additional shrinkage of approximately 4 % and 12 % occurring in terms of the pattern height in the porogen-free and porogen-loaded, respectively. Surprisingly though, Figure 3c and d indicate almost no change in the pattern width upon vitrification. For some reason lateral shrinkage is not observed after the patterns are removed from the mold and vitrified. While we do not completely understand the apparent lack of lateral shrinkage, these observations are consistent with simulations on the shrinkage of UV curable resists in nanoimprint molds; upon cross-linking they also shrink in the height direction without significant changes in the pattern width.[26]

The k of the imprinted materials can be estimated from the measured Q_c^2 values. From Figure 2d, the Q_c^2s of the residual layer for the porogen-free and porogen-loaded samples are 5.01×10^{-4} Å^{-2} and 5.50×10^{-4} Å^{-2}, respectively. The linear relationship between Q_c^2 and k (Fig. 1b) can be used to estimate $k = 2.46$ and $k = 2.68$ for the porous and non-porous patterns, respectively. Notice that the estimated k for the porous pattern is slightly higher than the target of 2.3 required for the ultralow-k mark. For some reason the dielectric constant is slightly higher than expected. However, the estimated k for the imprinted porogen-free pattern of 2.68 is slightly lower than the $k = 2.84 \pm 0.05$ reported for the unpatterned non-porous material.[18,19] It appears that the imprint process modifies the porosity (both intrinsic and induced) compared to the non-patterned planar films. This seems reasonable as imprinting induces large shear deformation fields into the material and increases the interfacial area; the microstructures of the vitrified pattern should be somewhat different. However a detailed investigation of how imprinting impacts the porosity is beyond the scope of this manuscript and the focus of a current investigation in our laboratory.

In conclusion, we have shown that nanoimprint lithography can be used to create patterned ILDs by directly imprinting a PMSQ-based organosilicate followed by vitrification. Patterns within a mold can be replicated with very high fidelity into a organosilicate material and this fidelity is maintained during the high temperature vitrification process. Only a modest amount of pattern shrinkage occurs and this shrinkage is primarily in the vertical direction. The changes in pattern width are minimal. Furthermore, these imprinted PMSQs can be made nanoporous through the use of a sacrificial porogen material. Generating the porosity does not appear to adversely affect the pattern quality in terms of shape or cross-section. It appears that the porosity of the patterns is *slightly* different from the same materials that have not gone through the patterning process and these differences are currently being explored in detail.

Experimental

Direct Patterning of PMSQs: The preparation of the PMSQ-based terpolymer is described elsewhere in detail [18,19]. Briefly, proper ratios of the three monomers methyltrimethoxysilane, 1,2-bis(triethoxysilyl)ethane, and dimethyldimethoxysilane were partially reacted in an acidic environment to form an oligomeric prepolymer. This prepolymer was condensed, solidified and then re-dissolved in 4-methy 2-pentanone. To make the porous sample, the Tetronic porogen was added to the solution at 20 % by volume relative to the PMSQ content. Thin Films of PMSQ with or without porogen were made by spin cast at 209 rad s^{-1} (2000 rpm) onto clean Si wafer with a native oxide surface. The imprint mold was a periodic silicon oxide line-space gratings structure, with approximately 1000 Å line widths on a 2000 Å pitch and 1700 Å line height. This mold was treated with a tri-

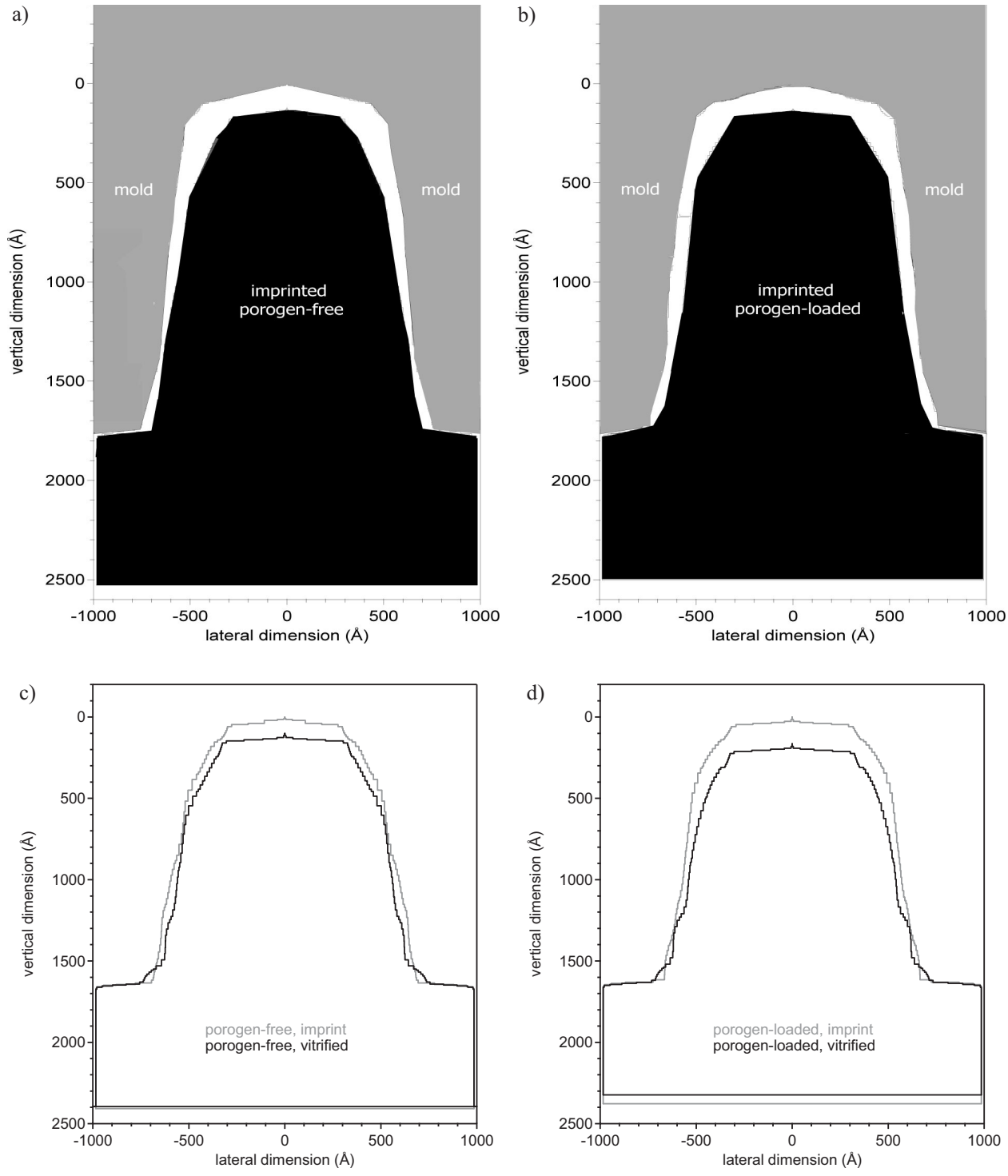

Figure 3. By combining the SLD profiles in Figure 2 with the CD-SAXS data, it is possible to quantify the average pattern cross-section of the imprinted patterns. In parts (a) and (b) the cross-section of the as-imprinted patterns are compared to the mold cross-section for both the porogen-free and porogen-loaded sample, respectively. This reveals shrinkage of the pattern from the original mold dimension in both the lateral and vertical directions. In parts (c) and (d) we see the pattern shape change upon vitrification for the same two patterns. Vitrification induces very minimal shrinkage in the lateral direction.

chloro(3,3,4,4,5,5,6,6,7,7,8,8,8-tridecafluorooctyl)silane vapor to facilitate the demolding process and directly placed on top of the as-cast films. The imprints were made under vacuum in two steps: 10 s at 170 °C and 1.4 MPa followed by 3 min at 200 °C and 3.4 MPa. The imprint tool was cooled to at least 55 °C before releasing the pressure and separating the mold from the pattern at room temperature. The as-imprinted patterns were further vitrified at 430 °C for 1 h in an inert nitrogen environment.

ADVANCED MATERIALS

Specular X-Ray Reflectivity (SXR) Measurement: SXR measurements were performed on a Philips X'PERT diffractometer using Cu Kα X-ray radiation ($\lambda = 1.54$ Å). The incident beam is focused with a curved mirror into a 4-bounce Ge [220] crystal monochromator before being incident onto the sample. The reflected beam is further conditioned with a 3-bounce Ge [220] crystal monochromator ensure the specular condition. The angular reproducibility of the goniometers that control the sample rotation and angular position of X-ray detector was 0.0001°. The reflectivity was collected at 25 °C under vacuum for all samples.

Positron Annihilation Lifetime Spectroscopy (PALS): PALS measurements were performed on the non-patterned version (planar films) of porous material in the vacuum chamber of an electrostatically-focused positron beam with ^{22}Na as the radioactive source of positrons. The positron beam energy was varied between 0.55 and 2.7 keV to control the implantation depth of the positrons into the films. This energy range corresponds to a mean implantation depth of 10 to 150 nm based on a film density of 1.0 g cm^{-3}. The lifetime spectra were fitted using both discrete and continuum fitting programs, i.e., POSFIT and CONTIN, to resolve positron/positronium lifetimes and intensities and pore size distribution (PSD).

Received: December 14, 2006
Revised: February 21, 2007
Published online: August 29, 2007

[1] S. Y. Chou, P. R. Krauss, P. J. Renstrom, *Appl. Phys. Lett.* **1995**, *67*, 3114.
[2] S. Y. Chou, P. R. Krauss, P. J. Renstrom, *Science* **1996**, *272*, 85.
[3] L. J. Guo, *J. Phys. D* **2004**, *37*, R123.
[4] S. Y. Chou, P. R. Krauss, *Microelectron. Eng.* **1997**, *35*, 237.
[5] M. D. Austin, H. Ge, W. Wu, M. Li, Z. Yu, D. Wasserman, S. A. Lyon, S. Y. Chou, *Appl. Phys. Lett.* **2004**, *84*, 5299.
[6] F. Hua, Y. Sun, A. Guar, M. A. Meitl, L. Bilhaut, L. Rotkina, J. Wang, P. Geil, M. Shim, J. A. Rogers, *Nano Lett.* **2004**, *4*, 2467.
[7] X.-M. Yan, S. Kwon, A. M. Contreras, J. Bokor, G. A. Somorjai, *Nano Lett.* **2005**, *5*, 745.
[8] S.-H. Park, T.-W. Lim, D.-Y. Yang, J.-H. Jeong, K.-D. Kim, K.-S. Lee, H.-J. Kong, *Appl. Phys. Lett.* **2006**, *88*, 203 105.
[9] D. S. Macintyre, Y. Chen, D. Lim, S. Thoms, *J. Vac. Sci. Technol. B* **2001**, *19*, 2797.
[10] M. D. Stewart, C. G. Willson, *MRS Bull.* **2005**, *30*, 947.
[11] G. M. Schmid, M. D. Stewart, J. Wetzel, F. Palmieri, J. Hao, Y. Nishimura, K. Jen, E. K. Kim, D. J. Resnick, A. Liddle, C. G. Wilson, *J. Vac. Sci. Technol. B* **2006**, *24*, 1283.
[12] S. Matsui, Y. Igaku, H. Ishigaki, J. Fujita, M. Ishida, Y. Ochiai, H. Namatsu, M. Komuro, *J. Vac. Sci. Technol. B* **2003**, *21*, 688.
[13] K.-i. Nakamatsu, K. Watanabe, K. Tone, T. Katase, W. Hattori, Y. Ochiai, T. Matsuo, M. Sasago, H. Namatsu, S. Matsui, *Jpn. J. Appl. Phys. Part 1* **2004**, *43*, 4050.
[14] H. J. H. Chen, J. F. Liu, Y. J. Hsu, J. C. C. Syu, F. S. Huang, *Nanotechnology* **2005**, *16*, 2913.
[15] K. Maex, M. R. Baklanov, D. Shamiryan, F. Iacopi, S. H. Brongersma, Z. S. Yanovitskaya, *J. Appl. Phys.* **2003**, *93*, 8793.
[16] M. Morgen, E. T. Ryan, J.-H. Zhao, C. Hu, T. Cho, P. S. Ho, *Annu. Rev. Mater. Sci.* **2000**, *30*, 645.
[17] R. D. Miller, *Science* **2001**, *286*, 421.
[18] D. Y. Yoon, H. W. Ro, E. S. Park, J.-K. Lee, H.-J. Kim, K. Char, H.-W. Rhee, D. Kwon, D. W. Gidley, *Mater. Res. Soc. Symp. Proc.* **2003**, *766*, 241.
[19] H. W. Ro, K. J. Kim, P. Theato, D. W. Gidley, D. Y. Yoon, *Macromolecules* **2005**, *38*, 1031.
[20] H.-J. Lee, C. L. Soles, H. W. Ro, R. L. Jones, E. K. Lin, W.-L. Wu, D. R. Hines, *Appl. Phys. Lett.* **2005**, *87*, 263 111.
[21] H.-J. Lee, H. W. Ro, C. L. Soles, R. L. Jones, E. K. Lin, W.-L. Wu, D. R. Hines, *J. Vac. Sci. Technol. B* **2005**, *23*, 3023.
[22] L. G. Parratt, *Phys. Rev.* **1954**, *95*, 359.
[23] J. F. Anker, C. F. Majkrzak, *Proc. SPIE-Int. Soc. Opt. Eng.* **1992**, *1738*, 260.
[24] R. L. Jones, R. L. T. J. Hu, E. K. Lin, W.-L. Wu, R. K. Kolb, D. M. Casa, P. Boulton, G. G. Barclay, *Appl. Phys. Lett.* **2003**, *83*, 4059.
[25] T. J. Hu, R. L. Jones, E. K. Lin, W.-L. Wu, D. Keane, S. Weigand, J. P. Quintana, *J. Appl. Phys.* **2005**, *96*, 1983.
[26] M. Colburn, I. Suez, B. J. Choi, M. Meissl, T. Bailey, S. V. Sreenivasan, J. G. Ekerdt, C. G. Wilson, *J. Vac. Sci. Technol. B* **2001**, *19*, 2685.

